Inorganic Chemistry

pubs.acs.org/IC

Featured Article

Exploring the Te(II)/Te(IV) Redox Couple of a Tellurorosamine Chromophore: Photophysical, Photochemical, and Electrochemical Studies

Nayanika Kalita, Matthew R. Crawley, Lauren E. Rosch, Owen Szeglowski, and Timothy R. Cook*

Cite This: *Inorg. Chem.* 2024, 63, 13157−13165

Read Online

ACCESS | Metrics & More | Article Recommendations | Supporting Information

ABSTRACT: A tellurorosamine dye [**Te(II)**] undergoes aerobic photooxidation. Although Te(IV) species have been used in a number of oxidations, key Te(IV)-oxo and Te(IV)-bis(hydroxy) intermediates are challenging to study. Under aerobic irradiation with visible light, **Te(II)** (λ_{max} = 600 nm) transforms into a Te(IV) species (λ_{max} = 669 nm). The resultant Te(IV) species is not stable in the dark or at −20 °C, decomposing back to **Te(II)** and other byproducts over many hours. To eliminate the structural ambiguity of the Te(IV) photoproduct, we used spectroelectrochemistry, wherein the bis(hydroxy) **Te(IV)-$(OH)_2$** was electrochemically generated under anaerobic conditions. The absorption of **Te(IV)-$(OH)_2$** matches that of the Te(IV) photoproduct. Because isosbestic points are maintained both photochemically and electrochemically, the oxo core formed photochemically must rapidly equilibrate with **Te(IV)-$(OH)_2$**. Calculations on the bis(hydroxy) versus oxo species further corroborate that the equilibration is rapid and the spectra of the two species are similar. To further explore Te(IV) cores, two novel compounds, **Te(IV)-Cl_2** and **Te(IV)-Br_2**, were synthesized. Characterization of **Te(IV)-X_2** was simplified because these cores have no analogue to the **Te(IV)-(O)/Te(IV)-$(OH)_2$** equilibrium. This work provides insights into the photophysical and electrochemical behavior of Te analogues of chalcogenoxanthylium dyes, which are relevant for a broad range of photochemical applications.

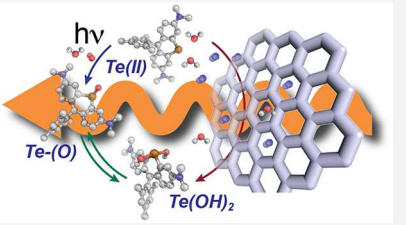

INTRODUCTION

Tellurium chalcogenides exhibit different photophysical behaviors and excited-state reactivities compared to their lighter O and S analogues. For example, they absorb light at longer wavelengths, they show enhancement in triplet quantum yields, they stabilize variable oxidation states, they form hypervalent compounds,[1−4] and they make unique supramolecular structures.[5−9] Most of these properties are attributed to tellurium's metalloid nature and its inherent tendency to induce the heavy-atom effect.[10] In addition, Te(II) sites in organotellurium compounds can also participate in noncovalent bonding interactions, have Lewis acid character, and have high polarizability.[10] These properties are attractive for a wide range of applications including catalysis,[11−13] photodynamic therapy,[14−18] optoelectronics,[19−21] and energy storage and conversion.[22−26]

Xanthylium dyes exhibit interesting characteristics, especially those containing heavier chalcogen atoms.[27−31] The first Te analogues of rosamine/rhodamine chromophores were reported in 2007 by Detty et al.[27] They have high oscillator strengths and generate singlet oxygen ($^1O_2$) when exposed to visible light. These molecules have been explored as photocatalysts for organic transformations like the oxidation of thiols to disulfides,[32] of phosphines to phosphine oxides,[33] of silanes to silanol,[33] and of tetrahydroisoquinolines to dihydroisoquinolines,[34] to name a few. They have also been explored as fluorescent probes for biological and materials science applications.[35−38] These transformations are purported to occur via a Te(II)/Te(IV) redox couple, as summarized in Scheme 1.[28,32,39] Te(II) cores react with $^1O_2$ to form a Te(IV)-peroxo complex, which subsequently reacts with a second

Scheme 1

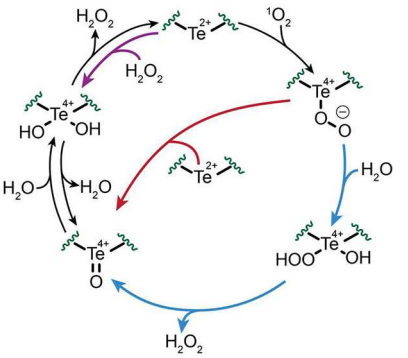

Received: March 15, 2024
Revised: June 26, 2024
Accepted: July 1, 2024
Published: July 11, 2024

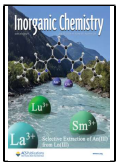

https://doi.org/10.1021/acs.inorgchem.4c01077
Inorg. Chem. 2024, 63, 13157−13165

Te(II) (red pathway) or water (blue pathway) to generate a Te(IV)-oxo species. In the presence of water, the oxo is in equilibrium with a bis(hydroxy) species. One way to close the cycle is the elimination of hydrogen peroxide (H_2O_2), which is invoked in some studies.[32] Alternatively, the Te(II) core can be regenerated upon oxidation of the substrate by the reactive Te(IV) intermediates shown in Figure 1, as described recently.[39]

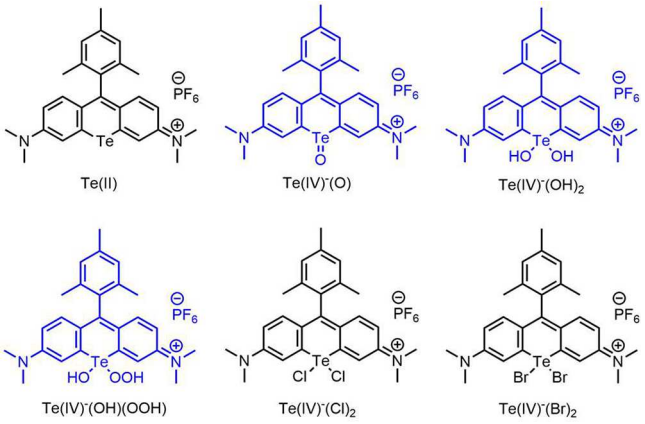

Figure 1. Structures of Te(II) and Te(IV) rosamines.

Some studies have suggested that H_2O_2 is generated as an elimination product during a thermal regeneration of Te(II) from Te(IV)-$(OH)_2$ at ∼61 °C.[28] However, there are underlying thermodynamic inconsistencies in this speculation. If the chemical oxidation of Te(II) to Te(IV) by H_2O_2 is thermodynamically favorable (purple pathway, Scheme 1),[28,29] the reverse reaction must be energetically uphill, yet there are reports of generating the Te(IV) core by the simple thermal reaction of Te(II) with H_2O_2.[28] The role of H_2O_2 is further obscured by the fact that it may also be generated during transformation of the proposed hydroxyperhydroxy complex of Te(IV) when it converts to the oxo, which is a key step of the blue pathway in Scheme 1.[32,34] Furthermore, these oxidized cores often show reactivity patterns similar to that of H_2O_2, so chemical assays for the latter may give false positives due to the presence of the former. Although electrochemical study of Te(II)/Te(IV) redox chemistry is not unprecedented,[23,40] it is underexplored in these xanthylium dyes.

As such, we were interested in understanding the nature of the Te(II)-to-Te(IV) transformation. We selected a xanthylium chromophore with a pendant mesitylene group for our studies, which was first reported in 2013.[28] We were interested in this dye due to its high quantum yield for $^1O_2$ (0.75) and because the mesitylene group provides extra stability by preventing the reactive 9′ position from an inter- or intramolecular nucleophilic attack. In addition to investigating the aerobic photochemical oxidation of **Te(II)** (see Figure 1 for structures and their abbreviations), we explored the electrochemical generation of Te(IV) cores. We also synthesized two novel compounds, the halogen adducts **Te(IV)-$(Cl)_2$** and **Te(IV)-Br_2**, with the expectation that they could help us to understand the electronic structure of the related Te(IV)-X_2 species, **Te(IV)-$(OH)_2$** (Scheme 2).

Scheme 2

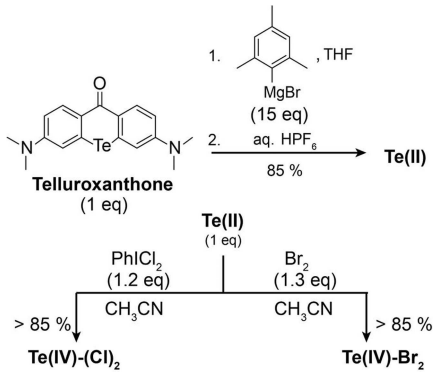

EXPERIMENTAL SECTION

Materials. Commercially available starting materials were used without further purification except diethylamine and tetramethylethylenediamine, which were freshly distilled over KOH prior to use. Solvents were purified using a Pure Process Technology Grubbs-style solvent system.

Methods. Photolysis experiments were carried out using a broadband GE 850 lm light-emitting-diode (LED) lamp. NMR spectra were acquired on INOVA-400, INOVA-500, or Bruker NEO-500 MHz instruments. All chemical shifts (δ) are reported in parts per million (ppm). For ^{1}H NMR, the signals were referenced against the residual proteo-solvent peaks. ^{125}Te NMR was acquired by operating the Bruker NEO-500 MHz instrument at 156 MHz. Mass spectrometry data were obtained using a Thermo Fischer Linear Ion Trap (LTQ) mass spectrometer. The mass spectrometer was set to electrospray ionization positive mode. UV−vis spectra were acquired in a quartz cuvette (path length = 1 cm) with an Agilent Cary 8454 UV−vis spectrophotometer. All of the electrochemical experiments were performed with a BioLogic SP-300 potentiostat/galvanostat under nitrogen gas. Data were acquired and processed using the *EC-Lab* software package. A 3.0-mm-diameter glassy carbon working electrode (CH instruments, USA), a Pt wire counter electrode (CH instruments, USA), and a nonaqueous $Ag/AgNO_3$ reference electrode were used. Tetra-*n*-butylammonium hexafluorophosphate ($TBAPF_6$) was recrystallized three times in 200-proof ethanol and dried in vacuo for more than 24 h prior to use. Ferrocene was used as an internal standard. Spectroelectrochemical experiments were performed under nitrogen using a Pine WaveDriver 40 potentiostat/galvanostat integrated with an Avantes AvaSpec UV−vis spectrophotometer. Data were acquired and processed in the *Aftermath* software package. A honeycomb Pt working electrode embedded with a Pt counter electrode and a pseudo-Ag wire reference electrode, compatible with the instrument, was used. UV−vis spectra were acquired in a quartz cuvette with a 1.7 mm path length. Parameters were set to 0.03 s integration time, boxcar width 10, and samples averaged to 50.

All geometry optimizations and frequency calculations of the relevant structures were performed in *Gaussian09* or *ORCA* with an acetonitrile (CH_3CN) solvent field. Coordinates to perform the calculations were adapted from the crystal structures of **Te(II)** and **Te(IV)-Cl_2** and modified as required. The absence of imaginary frequencies confirmed the convergence of geometry optimization calculations.

Crystallographic Details. Blue prismatic crystals of **Te(II)** were grown by slow diffusion of diethyl ether into a solution of **Te(II)** in CH_3CN. The datum crystal ($0.04 \times 0.07 \times 0.10$ mm^3) was mounted on a Rigaku XtaLAB Synergy diffractometer coupled to a Rigaku Hypix detector with Mo Kα radiation (λ = 0.71073 Å) from a PhotonJet microfocus X-ray source at 101 K. The diffraction images were processed and scaled using the *CrysAlisPro* software.[41] Data were truncated at 0.78 Å, which allowed for an overall I/σ of 14.3. During the preparation of this paper, another paper by McCormick et al. also

https://doi.org/10.1021/acs.inorgchem.4c01077
Inorg. Chem. 2024, 63, 13157−13165

reported **Te(II)**.[39] When compared, the data sets are in strong agreement with one another. Single crystals of **Te(IV)-Cl$_2$** were grown by slow diffusion of diethyl ether into a solution of **Te(II)** in CH_3CN. The green crystals were suspended in N-paratone oil, and the datum crystal (0.063 × 0.081 × 0.091 mm^3) was affixed to a glass fiber and mounted on a Huber three-circle diffractometer at the ChemMatCARS Beamline 15ID-D at the Advanced Photon Source housed at Argonne National Laboratory. A Si(111) monochromator was used to produce a 200 × 200 μm beam at 30 keV (0.41327 Å). Diffraction images were recorded on a Dectris Pilatus3 X 1M detector. The sample was cooled to 20 K using an open-flow liquid-helium cryostat. Data were integrated and scaled using the Bruker *APEX3* software package.[42] Data were truncated at 0.50 Å, which provided an overall I/σ of 39.6. Structure solution was performed using *SHELXT*[43] and least-squares refinement using *SHELXL*[44] with the *OLEX2* software package.[45] For both structures, structure solution and refinement was routine, with no signs of disorder or problematic diffraction data.

Synthesis of Te(II). The procedure to synthesize **Te(II)** was adapted from the literature.[28,46] A solution of 3-bromomagnesium mesitylene in tetrahydrofuran (THF; 15.0 equiv) was added dropwise to a stirred solution of 3,6-bis(dimethylamino)-9*H*-telluroxanthen-9-one (100 mg, 1.0 equiv) in THF (20 mL) under a nitrogen atmosphere. The reaction mixture was refluxed at 65 °C for 18 h. The color darkened from orange-yellow to orange as the originally opaque solution turned transparent over the course of 18 h. The solution was then cooled to room temperature, and 0.3 mL of glacial acetic acid was added. The orange color of the solution turned blue. The reaction mixture was poured into an Erlenmeyer flask covered with aluminum foil, containing 40 mL of 10% HPF_6 solution, and stirred overnight under aerobic conditions. The precipitated product was washed with water and diethyl ether to give 130 mg of solid. ^{1}H NMR (500 MHz, CD_2Cl_2): δ 7.51 (m, 4 H), 7.06 (s, 2 H), 6.75 (dd, 2 H), 3.22 (s, 12 H), 2.42 (s, 3 H), 1.83 (s, 6 H). ^{125}Te NMR (156 Hz, CD_3OD): δ 732.68. λ_{max} in CH_3CN = 600 nm (ε = 8.2 × 10^4 M^{-1} cm^{-1}).

Synthesis of Te(IV)-Cl$_2$. A stirred solution of dicholoroiodobenzene ($PhICl_2$; 6.89 mg, 1.1 equiv) in 4 mL of CH_3CN was added dropwise to a solution of **Te(II)** (15.02 mg, 1.0 equiv) in 8 mL of CH_3CN under ambient conditions. The reaction mixture immediately changed from blue to green and was stirred for 5 min. The solvent was removed by vacuum, and the resulting solid was washed with petroleum ether and recrystallized in CH_3CN−diethyl ether to obtain purple crystals. ^{1}H NMR (500 MHz, CD_3OD): δ 8.12 (br s, 2 H), 7.31 (d, J = 10.0 Hz, 2 H), 7.10 (s, 2 H), 6.91 (dd, J = 10.0 and 5.0 Hz, 2 H), 3.43 (s, 12 H), 2.41 (s, 3 H), 1.97 (s, 6 H). ^{125}Te NMR (156 Hz, CD_2Cl_2): δ 591.59. λ_{max} in CH_3CN = 668 nm (ε = 8.5 × 10^4 M^{-1} cm^{-1}); m/z 569.24 (calcd for $C_{26}H_{29}Cl_2N_2Te^+$: m/z 569.08). Elem anal. Calcd for $C_{26}H_{29}Cl_2N_2Te{\cdot}C_2H_5OH$: C, 44.31; H, 4.65; N, 3.69. Found: C, 44.27; H, 4.46; N, 4.06.

Synthesis of Te(IV)-Br$_2$. From a stock solution of Br_2 in CH_3CN, 1.3 equiv (2.0 μL) of Br_2 was pipetted out and dissolved in 5 mL of CH_3CN. The diluted Br_2 solution was added dropwise to a stirred solution of **Te(II)** (20.0 mg, 1.0 equiv) in 5 mL of CH_3CN under ambient conditions. The reaction mixture changed from blue to green and was stirred for 5 min. The solvent was removed by vacuum, and the resulting solid was washed with petroleum ether and recrystallized in CH_3CN−diethyl ether to obtain golden green crystals. ^{1}H NMR (500 MHz, CD_3OD): δ 8.14 (d, J = 5.0 Hz, 2 H), 7.31 (d, J = 10.0 Hz, 2 H), 7.10 (s, 2 H), 6.91 (dd, J = 10.0 and 5.0 Hz, 2 H), 3.43 (s, 12 H), 2.41 (s, 3 H), 1.98 (s, 6 H); λ_{max} in CH_3CN = 668 nm (ε = 8.6 × 10^4 M^{-1} cm^{-1}); m/z 659.06 (calcd for $C_{26}H_{29}Br_2N_2Te^+$: m/z 658.97). Elem anal. Calcd for $C_{26}H_{29}Br_2N_2Te{\cdot}CH_2Cl_2$: C, 36.57; H, 3.52; N, 3.16. Found: C, 36.49; H, 3.59; N, 3.27.

RESULTS AND DISCUSSION

Photophysics and Photochemistry. Solutions of **Te(II)** can undergo aerobic photooxidation to generate Te(IV) species when irradiated with visible light. The major absorption band of Te(II) has a λ_{max} at 600 nm with a shoulder at 560 nm. In CH_3CN solvent, the molar absorption coefficient of **Te(II)** is 8.2 × 10^4 M^{-1} cm^{-1} at 600 nm (Figure 1). When a sample of **Te(II)** was dissolved in 10% (v/v) H_2O in CH_3CN solvent and irradiated, the band at 600 nm decreased with a concomitant rise at 669 nm. Three well-maintained isosbestic points were observed at 362, 467, and 621 nm (Figure 2). Photochemistry from **Te(II)** to **Te(IV)-(OH)$_2$** also occurred in 1:4 H_2O−CH_3OH solutions (Figure S7). When irradiation was carried out in CH_3CN with no water, the Te(II) band at 600 nm also decreased, but rather than a growth at 669 nm, a band at 660 nm was observed.

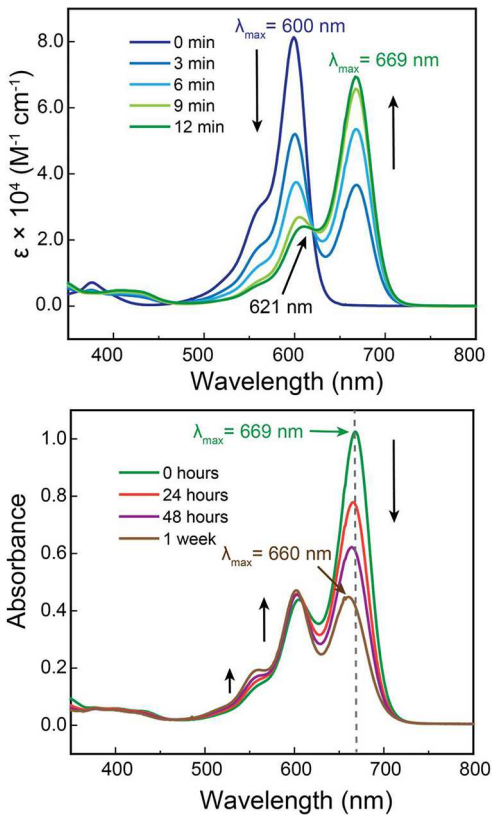

Figure 2. Top: Aerobic photooxidation of **Te(II)** to **Te(IV)-(OH)$_2$** in CH_3CN with 10% H_2O solvent, irradiated with a broadband LED light at room temperature. Bottom: Degradation of **Te(IV)-(OH)$_2$** stored at −20 °C in the dark over time. The dashed line represents a blue shift in λ_{max}.

Because the photochemistry was not clean under water-free conditions (Figure S8), there is strong evidence that the blue pathway that passes through **Te(IV)-(OH)(OOH)** is operative. This intermediate then eliminates H_2O_2 to give **Te(IV)-(O)**, which rapidly equilibrates with **Te(IV)-(OH)$_2$** via the addition of water. If the red pathway of Scheme 1 was dominant, photochemistry in the absence of water would culminate in the quantitative formation of **Te(IV)-(O)**. Although this Te(IV) core is reactive with certain substrates, it is not expected to rapidly self-decompose. In fact, because it is in equilibrium with **Te(IV)-(OH)$_2$** when water is present, if the oxo core was unstable, mixtures of bis(hydroxy) and oxo would quickly degrade. Instead, for standing solutions of **Te(IV)-(OH)$_2$/Te(IV)-(O)**, equilibrium mixture change slowly once they are no longer actively irradiated (Figure S8). Over the course of 48 h, the band at 669 nm decreased and shifted to ∼660 nm. Although there is some recovery of

https://doi.org/10.1021/acs.inorgchem.4c01077
Inorg. Chem. 2024, 63, 13157−13165

the band at 600 nm that is associated with **Te(II)**, there is a third band at 550 nm that tails into the other features and could be responsible for the shift from 669 to 660 nm of the Te(IV) species. Thus, this thermal decomposition is not a simple conversion of **Te(IV)-$(OH)_2$** back to **Te(II)**. The species that gives rise to absorption at 550 nm is also observed during photolysis in CH_3CN when no water is present. The appearance of other absorption features is indicative of side reactions that could result from the highly reactive nature of the Te(IV) species. Attempts to prevent thermal decomposition of **Te(IV)-$(OH)_2$**/**Te(IV)-(O)** at lower temperatures (∼−20 °C) still resulted in spectral changes. A significant amount of **Te(IV)-(OH_2)** converted back to **Te(II)** and the side product that gives rise to an absorption at 550 nm (Figure 2).

NMR Investigations. Aerobic photooxidation of a 3.9 mM solution of **Te(II)** was carried in 25% D_2O in CD_3OD. Figures 3 and S10 illustrate the aromatic region of NMR spectra

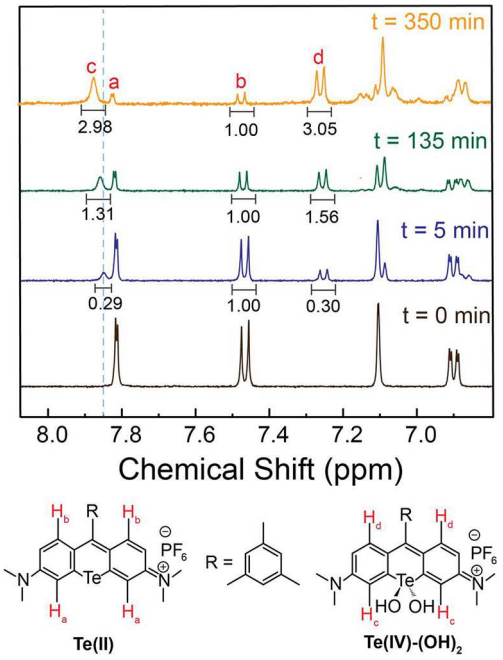

Figure 3. Top: Aromatic region of the ^1H NMR spectrum of **Te(II)** after t = 0, 5, 135, and 350 min of irradiation in CD_3OD with 25% D_2O under aerobic conditions.

recorded at different times. As seen from the stacked NMR spectra, new peaks grew at 7.85 (br s), 7.25 (d), 7.09 (s), and 6.87 (dd) ppm, indicating the conversion of **Te(II)** to a **Te(IV)-$(OH)_2$**/**Te(IV)-(O)** mixture. The peaks at 7.81 and 7.47 ppm at t = 0 min were assigned to protons **a** and **b** of **Te(II)**, while the peaks at 7.85 and 7.25 ppm were assigned to protons **c** and **d** of the oxidized species. The peaks of the oxidized cores are more broad than those attributed to Te(II), which could be due to the rapid equilibration between **Te(IV)-$(OH)_2$** and **Te(IV)-(O)** and complicates quantification of the relative amounts of two Te(IV) species. Nonetheless, because these protons are three and four bonds away from the Te center, respectively, any change in the Te environment would be expected to alter the chemical environment of these protons more prominently than the others. The progress of the reaction was monitored by observing the relative intensities of peaks **b** and **d**. Approximately, 75% conversion was achieved after 350 min of irradiation. Beyond 350 min, the reaction mixture starts to degrade without going into completion, as indicated by the NMR spectra (Figure S10).

Electrochemistry. To explore the Te(II)/Te(IV) redox couple in these compounds, we carried out electrochemical studies of **Te(II)** (Figure 4). We hypothesized that **Te(IV)-$(OH)_2$** is electrochemically accessible by the two-electron oxidation of **Te(II)**, followed by the coordination and deprotonation of two water molecules, furnishing **Te(IV)-$(OH)_2$**. Figure 4 shows the cyclic voltammetry (CV) curve of **Te(II)** in 1:9 H_2O:CH_3CN.

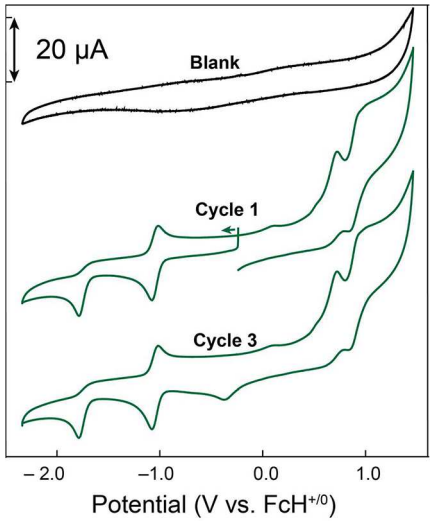

Figure 4. CV curves of a 1 mM solution of **Te(II)** in CH_3CN with 10% H_2O solvent at 50 mV/s under nitrogen. WE = glassy carbon, RE = 10 mM $AgNO_3$ solution, CE = platinum wire, and SE = 100 mM $TBAPF_6$. Ohmic IR compensated. IUPAC convention. A three-electrode system where the WE was not separated from the CE was employed. The potential values were standardized against the ferrocene−ferrocenium couple ($FcH^{+/0}$).

The event at 0.74 V was assigned to an electrochemically quasi-reversible two-electron oxidation of **Te(II)**, generating **Te(IV)-$(OH)_2$**. Such two-electron oxidations of Te(II) to Te(IV) are seen in other Te heterocycles as well.[47] The event at 0.92 V was assigned to further oxidation chemistry of the Te(IV) core. The events at −1.0 and −1.8 V were attributed to additional ring-centered reduction chemistry, in analogy to what has been observed for previous Te systems, as well as simple O-containing rhodamines.[47,48] Differential pulse voltammetry (DPV; Figure S12) and spectroelectrochemical data (see below) corroborate our findings from the CV studies. A reduction event appears at −0.38 V, which was associated with the regeneration of **Te(II)** from **Te(IV)-$(OH)_2$**/**Te(IV)-(O)**. The disappearance of this feature at slower scan rates implies a chemical transformation involving **Te(IV)-$(OH)_2$**, **Te(IV)-(O)**, or both (Figures S12 and S13). Our electrochemical findings substantiate the earlier conclusions regarding the relatively unstable nature of equilibrium mixtures of **Te(IV)-$(OH)_2$**/**Te(IV)-(O)**.

To further investigate the Te(II)/Te(IV) redox couple, CV curves of structurally similar **Te(IV)-$(Cl)_2$** and **Te(IV)-$(Br)_2$** were obtained (Figure 5) by the straightforward oxidation of the Te(II) core with either $PhICl_2$ or Br_2. A prominent reduction feature was observed at −0.51 V for **Te(IV)-$(Cl)_2$** and at −0.41 V for **Te(IV)-$(Br)_2$**. These events were assigned

https://doi.org/10.1021/acs.inorgchem.4c01077
Inorg. Chem. 2024, 63, 13157−13165

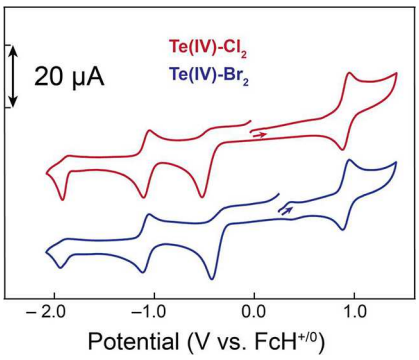

Figure 5. CV curves of **Te(IV)-(Cl)$_2$** and **Te(IV)-(Br)$_2$** (in CH_3CN) at 50 mV/s under nitrogen. WE = glassy carbon, RE = 10 mM $AgNO_3$ solution, CE = platinum wire, and SE = 100 mM $TBAPF_6$. Ohmic IR compensated. IUPAC convention. A three-electrode system where the WE was not separated from the CE was employed. The potential values were standardized against $FcH^{+/0}$.

to the reduction of **Te(IV)-Cl$_2$** and **Te(IV)-Br$_2$** to **Te(II)**. Based on the CV responses, it appears that all three Te(IV) cores can undergo reductive transformations to Te(II), where the redox change of the tellurium prompts ejection of the X-type ligands (Figure 4, cycle 3).

UV−Vis Spectroelectrochemistry. To draw a parallel between the photochemical and electrochemical behavior of Te(II) and Te(IV) species, we used UV−vis spectroelectrochemical techniques. The Te(II)-to-Te(IV) transition is accompanied by a characteristic change in absorption. On sweeping toward oxidizing potentials, the major absorption band of **Te(II)** at 600 nm started to disappear as a new absorption band with a λ_{max} value between 665 and 685 nm appeared. The λ_{max} values corresponding to the Te(IV) species generated under different conditions are summarized in Table 1.

Table 1. λ_{max} of Electrochemically Generated Te(IV)

solvent	λ_{max} (nm)
5% H_2O in CH_3CN	678
20% H_2O in CH_3CN	677
CH_3CN	682
sodium butoxide in CH_3CN	665
10% pyridine in CH_3CN	674

In a 1:9 H_2O:CH_3CN solvent, **Te(II)** transforms into a Te(IV) core with an isosbestic point at 621 nm and λ_{max} at 677 nm. Figure 6 illustrates the change in the UV−vis spectra during scanning over the potential region of interest, involving Te(II)/Te(IV) redox couples. The major absorption bands of the photochemically and electrochemically generated Te(IV) species match each other very closely (Figure S14). There are small spectral shifts, which we hypothesized are due to the presence of a supporting electrolyte. Because **Te(IV)-(OH)$_2$**/**Te(IV)-(O)** are reactive species, we explored the spectral shifts using **Te(IV)-Cl$_2$**, which shares a similar spectral profile and is also sensitive to solvent conditions. A solution of **Te(IV)-Cl$_2$** was made in a 1:9 H_2O−CH_3CN mixture, i.e., the photochemical conditions. The UV−vis spectra recorded before and after the addition of $TBAPF_6$ to the sample solution reveal that, as the supporting electrolyte is added, a minor red shift in absorption occurs. When the concentration of $TBAPF_6$ in the **Te(IV)-Cl$_2$** solution reached 100 mM, which matches the

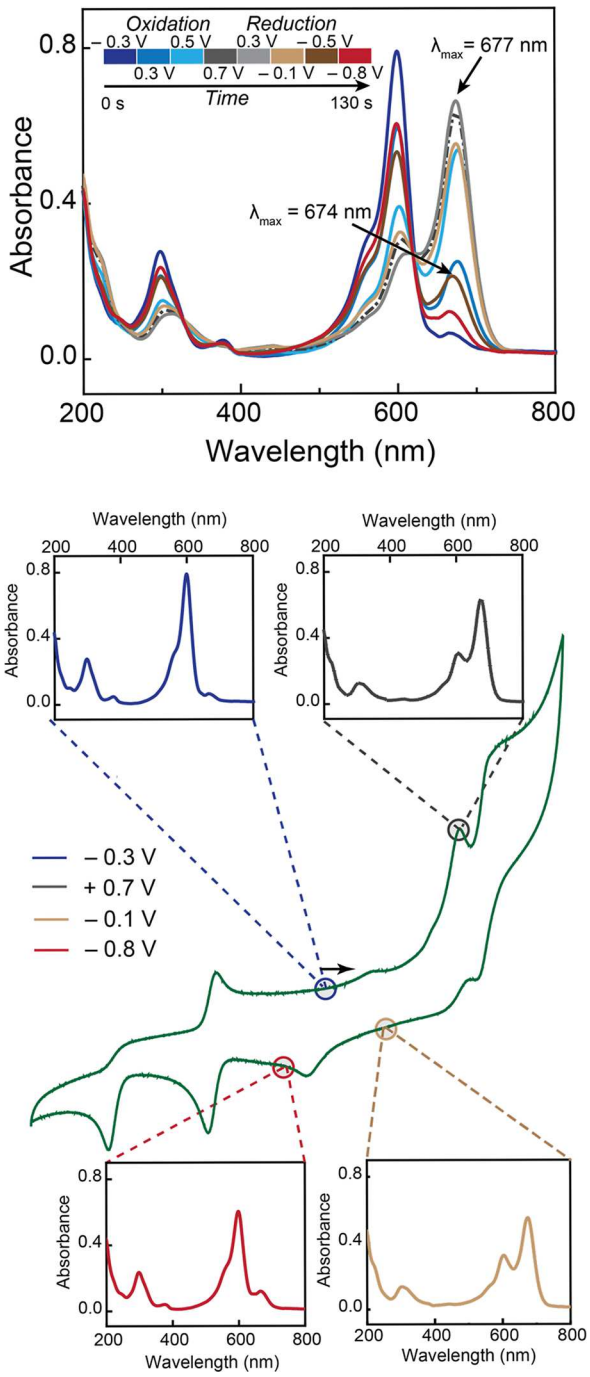

Figure 6. UV−vis spectroelectrochemical data of **Te(II)** in CH_3CN with 10% H_2O solvent in 100 mM $TBAPF_6$ at 50 mV/s under nitrogen. WE = Pt, RE = pseudo Ag wire, and CE = Pt. The WE was embedded with the CE. IUPAC convention. Top: Isosbestic conversion of **Te(II)** to **Te(IV)-(OH)$_2$**. Bottom: Isolated UV−vis spectra at different potentials.

electrochemistry conditions, the red shift in λ_{max} reached ∼5 nm, similar to the ∼8 nm shift of the **Te(IV)-(OH)$_2$** dye (Figure S19). Thus, we conclude that the photochemically generated Te(IV) arrives at the same equilibrium mixture as the electrochemically generated Te(IV). Photochemically, **Te(IV)-(O)** is first formed and equilibrates with bis(hydroxy). Electrochemically, **Te(IV)-(OH)$_2$** is formed and rapidly equilibrates with oxo. The complementary routes to the **Te(IV)-(OH)$_2$**/**Te(IV)-(O)** equilibrium that both maintain

https://doi.org/10.1021/acs.inorgchem.4c01077
Inorg. Chem. 2024, 63, 13157−13165

isosbestic points indicate that the conversions between species are rapid, but this does not provide any information about which species is dominant.

The amount of **Te(IV)-(OH)$_2$** generated electrochemically was correlated with the amount of water present in the system, as seen from the normalized intensities of the peaks with 5% and 20% H_2O in CH_3CN (Figure S15). Because **Te(II)** is poorly soluble in water, a solution of **Te(II)** separates into a biphasic system over time at higher concentrations of H_2O in CH_3CN. Hence, relative intensities above 20% were not taken into consideration. A blue shift in λ_{max} of **Te(IV)-(OH)$_2$**/**Te(IV)-(O)** to 674 nm was observed (Figure 6), which was consistent with the photochemical experiments. During a reverse scan toward the Te(IV)/Te(II) redox couple, the reappearance of the major absorption band at 600 nm confirmed regeneration of **Te(II)**. We noticed that **Te(II)** formed a Te(IV) species in CH_3CN even when no water was present. We suspected that a CH_3CN adduct, **Te(IV)-(CH$_3$CN)$_2$**, was responsible for the observed behavior. Although such a coordination of solvent molecules is not very common, Te heterocycles with π-extended conjugation systems have shown similar behavior in tellurophenes.[49] Polar solvent molecules like CH_3CN can stabilize the electron-deficient Te(IV) center.

Depending on the quantity of water present in the system, there could be a competitive reaction, leading to the formation of either a **Te(IV)-(OH)$_2$** or **Te(IV)-(CH$_3$CN)$_2$** adduct. This may account for the 1 nm disparity in λ_{max} of the solutions containing 5% and 20% water in CH_3CN. The λ_{max} value of **Te(IV)-(CH$_3$CN)$_2$** appeared at 682 nm, and an isosbestic point was observed at 621 nm as the Te(II) core reacted. Upon the addition of 100 equiv of sodium butoxide to a 10^{-5} M solution of **Te(II)** in CH_3CN, the λ_{max} value and isosbestic point shifted to 665 and 618 nm, respectively (Figure S16). Due to the stronger Lewis base character of alkoxides, it was expected that they would substitute for the CH_3CN ligands, most likely forming a bis(butoxide) adduct of Te(IV). This suggests a similar behavior in the presence of water molecules, substantiating the evidence for the formation of **Te(IV)-(OH)$_2$**. Additionally, UV−vis spectra recorded in CH_3CN and in a mixture of H_2O−CH_3CN were significantly different following the first oxidation event (Figure S17). In CH_3CN, a new absorption feature started to appear at 508 nm and disappeared on the reverse scan. When water was present in the system, a broad absorption feature appeared between 400 and 600 nm. The dissimilarity in the absorption trends at higher oxidation potential supported the formation of different species in the presence and absence of water in CH_3CN. Figure S18 shows the change in absorption upon the reduction of **Te(II)** in the presence of water. No change was observed until the one-electron redox event. Spectroelectrochemical data obtained during the reduction of **Te(IV)-(Cl)$_2$** and **Te(IV)-Br$_2$** show regeneration of the parent dye molecule, **Te(II)**.

Structural Analysis. Single-crystal X-ray diffraction was used to determine the atomic connectivities. For both **Te(II)**, for which an earlier structure was recently reported[39] and **Te(IV)-Cl$_2$**, the expected planar diaminotelluroxanthylium core was found in the density map, with the mesityl group rotated out of plane along with an outer-sphere PF_6^- counterion to maintain charge neutrality (Figure 7). In the case of **Te(II)**, the mesityl group was found to be nearly perpendicular to the telluroxanthylium core with a dihedral angle of 90.60°. A bond-length comparison of the heterocyclic

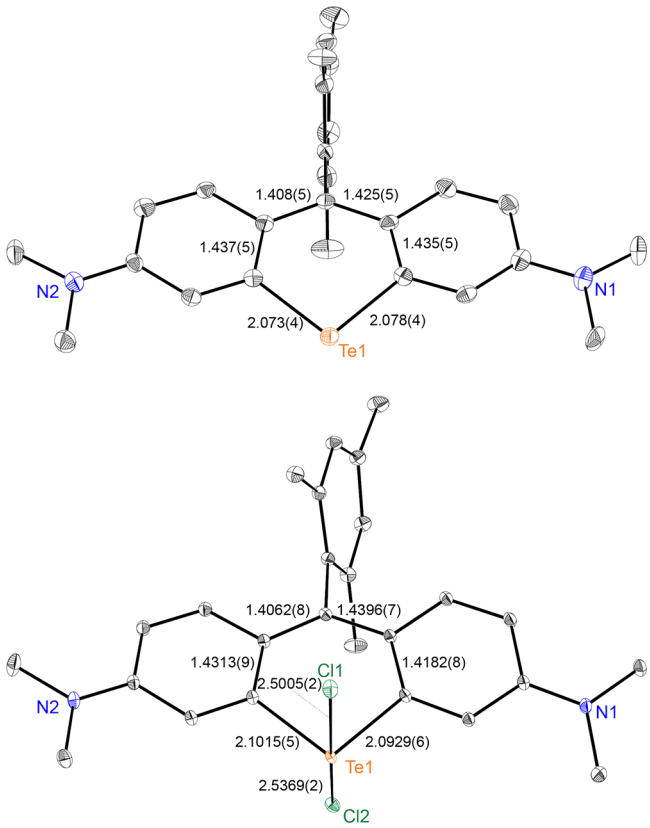

Figure 7. Structures of **Te(II)** (top) and **Te(IV)-Cl$_2$** (bottom) determined by single-crystal X-ray diffraction at 101 and 20 K, respectively. For both structures, the ellipsoid probability levels have been set at 50%. All bond lengths are reported in angstroms. H atoms and PF_6 counterions have been removed for clarity.

rings of **Te(II)** and **Te(IV)-Cl$_2$** can be found in Figure 7. **Te(IV)-Cl$_2$** possessed two axial chloro ligands roughly perpendicular to the plane of the telluroxanthylium core, resulting in a seesaw geometry at the Te center. The Cl1−Te1−Cl2 angle was found to be 169.11(1)°, while the C1−Ti1−C5 angle was 95.15(2)°, which is in agreement with the Te(II) C1−Te1−C5 angle of 95.0(1)°. Notably there is a statistically relevant disparity between the two Te−Cl bonds: Te1−Cl1 was found to be 2.5005(2) Å, while Te1−Cl2 was found to be 2.5369(2). Inspection of the molecular packing reveals two formula units of **Te(IV)-Cl$_2$** packed in a "head-to-head" orientation such that Te1 and Cl2 of adjacent unit cells are separated by 3.401 Å (Figure S21), whereas Cl1 is positioned such that no such interaction occurs. We therefore postulate that the difference in the Te−Cl bonds is a result of packing effects. Similarly, the mesityl group of **Te(IV)-Cl$_2$** is significantly canted compared to that of **Te(II)**; when packed, it is clear that interactions with adjacent dimethylamino groups result in this deviation. The telluroxanthylium core of **Te(IV)-Cl$_2$** shows greater deviation from planarity with a plane normal angle of 9.94° (planes generated by the carbon atoms of the two peripheral all-carbon six-membered rings) versus 5.21° for Te(II).

Computational Studies. Although some computational investigations have been carried out to understand the Te(II)/Te(IV) photochemistry and redox chemistry,[32,34] researchers were particularly interested in the equilibrium between the **Te(IV)-(OH)$_2$** and **Te(IV)-(O)** species and subsequent

https://doi.org/10.1021/acs.inorgchem.4c01077
Inorg. Chem. 2024, 63, 13157−13165

reaction to form **Te(II)**. Gibbs free energies ($\Delta G°$) were calculated from the balanced chemical reaction by using the energy values obtained from frequency calculations, as summarized in Table S1. Depending on the level of theory and basis sets, the energies of the two species varied but remained within 6 kcal/mol. The small energy difference suggests that neither **Te(IV)-(OH)$_2$** nor **Te(IV)-(O)** dominates at equilibrium. This is consistent with our broadened NMR peaks and the similar spectra for photochemical versus electrochemical oxidation, which would arrive at the equilibrium mixture from two different directions. If the oxidation chemistry of the **Te(IV)** cores originates from **Te(IV)-(O)**, as invoked in prior studies,[32,39] the ability of **Te(IV)-(OH)$_2$** to covert to oxo is important to continually replenish this species from the total pool of Te(IV).

The formation of **Te(IV)-(OH)$_2$** from the reaction of **Te(II)** with H_2O_2 is energetically favored, as evidenced by the significantly high negative value of ΔG and experimental oxidation of **Te(II)** with H_2O_2 to form a Te(IV) core.[28] This indicates that the likelihood of thermal elimination of H_2O_2 from **Te(IV)-(OH)$_2$** to regenerate **Te(II)** is low and prior observations of this chemistry may have been obscured by further thermodynamic driving forces associated with the oxidation of solvent or other species rather than the authentic formation of H_2O_2.

Time-dependent density functional theory (TD-DFT) calculations were carried out on the optimized geometries to predict the absorption spectra of **Te(IV)-(O)** and **Te(IV)-(OH)$_2$** using the polarizable continuum solvation model. In general, the calculations overestimated the excitation energy, leading to a blue shift in the values of λ_{max}. Such behavior is common for similar cyanine systems.[27,47,50,51] Theoretically predicted UV−vis spectra of **Te(IV)-(O)** and **Te(IV)-(OH)$_2$** resemble each other very closely (Figure S20); however, we found **Te(IV)-(OH)$_2$** to have a relatively higher molar absorption coefficient. This finding indicates that differentiating between the two species from their absorbance spectra alone is difficult. Figure 8 illustrates a qualitative description of the frontier molecular orbitals (FMOs) of **Te(IV)-(O)** and **Te(IV)-(OH)$_2$** and the calculated energy gap between the highest occupied molecular orbital (HOMO) and lowest unoccupied molecular orbital (LUMO) energy levels. Visualization of the FMOs indicate that the HOMOs of both **Te(IV)-(O)** and **Te(IV)-(OH)$_2$** were largely centered around the π-conjugated system with little participation from the mesitylene group, the Te atom, or the O atoms. The LUMO of **Te(IV)-(O)** had significant contribution from both the Te and O atoms, while the LUMO of **Te(IV)-(OH)$_2$** had a contribution only from the O atoms of the OH bonds. In LUMO, an increase in the electron density was observed at the C atom attached to the mesitylene group in all species. The major absorption band corresponding to the highest oscillator strength is a $\pi-\pi^*$ transition. The calculated HOMO−LUMO energy gaps in **Te(IV)-(O)** and **Te(IV)-(OH)$_2$** were found to be 2.2608 and 2.3580 eV, respectively.

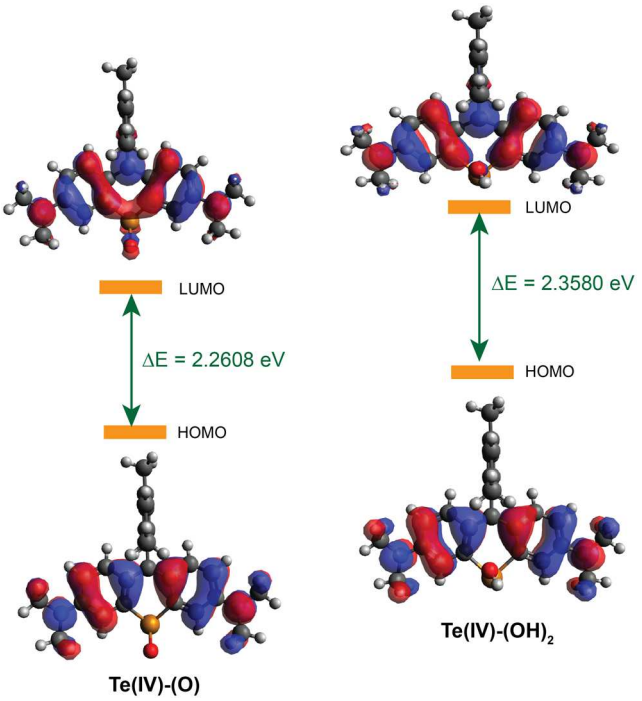

Figure 8. FMOs showing the relative lowering of energy and the HOMO−LUMO energy gap in **Te(IV)-(O)** and **Te(IV)-(OH)$_2$**.

CONCLUSION

Tellurorhodamine chromophores have several potential applications, but challenges remain in their effective integration that largely stem from the reactivity and stability differences of such compounds relative to their lighter analogues. The photophysics and photochemistry of these molecules are linked as their use as dyes is at odds with their self-sensitization in the presence of molecular oxygen. Furthermore, structural distortions that occur when replacing smaller O and S with Te further promote the reactivity of these species.

In this study, we have studied complementary routes to an oxidized mesitylene-functionalized tellurorosamine chromophore to better understand the photochemistry associated with the self-sensitization and subsequent reactivity of Te-containing xanthylium dyes. An analysis of our results along with prior descriptions of this chemistry support a pathway wherein **Te(II)** combines with $^1O_2$ to form a Te(IV)-peroxy that is highly reactive. When water is present, it rapidly coverts to a **Te(IV)-(OH)(OOH)** species, but in the absence of water, it quickly decomposes. An elimination of H_2O_2 from **Te(IV)-(OH)(OOH)** furnishes **Te(IV)-(O)**, an oxo core that equilibrates with **Te(IV)-(OH)$_2$**. This equilibration occurs faster than steady-state UV−vis measurements. We also access the **Te(IV)-(OH)$_2$/Te(IV)-(O)** equilibrium mixture by the direct oxidation of Te(II) to Te(IV), which generates **Te(IV)-(OH)$_2$** in water to feed the equilibrium mixture. Computational results suggest that neither **Te(IV)-(OH)$_2$** nor **Te(IV)-(O)** dominates at equilibrium because their energies are similar. These similarities extend to their absorption spectra, which were predicted by TD-DFT. Our findings were substantiated by characterizing related **Te(IV)-Cl$_2$** and **Te(IV)-Br$_2$** species, which do not have a corresponding equilibrium with an oxo analogue, simplifying their chemistry. Because conversion of **Te(II)** to **Te(IV)-X$_2$** can be easily carried out under ambient conditions with suitable oxidants ($PhICl_2$, Br_2, and H_2O_2), it implies that the reverse reactions are uphill, and the regeneration of **Te(II)** does not occur through a simple thermal elimination of X_2 (i.e., Cl_2, Br_2, and H_2O_2). Further interrogation of the **Te(IV)-(OH)$_2$/Te(IV)-(O)** equilibration using transient absorption spectroscopy is underway.

https://doi.org/10.1021/acs.inorgchem.4c01077
Inorg. Chem. 2024, 63, 13157−13165

■ ASSOCIATED CONTENT

Supporting Information

The Supporting Information is available free of charge at https://pubs.acs.org/doi/10.1021/acs.inorgchem.4c01077.

NMR spectroscopy, UV−vis spectroscopy, electrochemistry, UV−vis spectroelectrochemistry, and crystallography and computational details (PDF)

Accession Codes

CCDC 2254806 and 2254807 contain the supplementary crystallographic data for this paper. These data can be obtained free of charge via www.ccdc.cam.ac.uk/data_request/cif, or by emailing data_request@ccdc.cam.ac.uk, or by contacting The Cambridge Crystallographic Data Centre, 12 Union Road, Cambridge CB2 1EZ, UK; fax: +44 1223 336033.

■ AUTHOR INFORMATION

Corresponding Author

Timothy R. Cook − *Department of Chemistry, University at Buffalo, The State University of New York, Buffalo, New York 14260, United States;* orcid.org/0000-0002-7668-8089; Email: trcook@buffalo.edu

Authors

Nayanika Kalita − *Department of Chemistry, University at Buffalo, The State University of New York, Buffalo, New York 14260, United States*

Matthew R. Crawley − *Department of Chemistry, University at Buffalo, The State University of New York, Buffalo, New York 14260, United States;* orcid.org/0000-0002-2555-9543

Lauren E. Rosch − *Department of Chemistry, University at Buffalo, The State University of New York, Buffalo, New York 14260, United States;* orcid.org/0000-0002-6478-6415

Owen Szeglowski − *Department of Chemistry, University at Buffalo, The State University of New York, Buffalo, New York 14260, United States*

Complete contact information is available at: https://pubs.acs.org/10.1021/acs.inorgchem.4c01077

Funding

This work was supported by National Science Foundation (NSF) Award 1800288 (to T.R.C.). Characterization work was performed in part in the Chemistry Instrument Center (CIC), University at Buffalo, SUNY, Buffalo, NY. The Bruker AVANCE NEO500 MHz NMR was purchased with NSF CHE-2018160, a part of the UB NMR center. Part of the computational work was performed at the University at Buffalo's Center for Computational Research.

Notes

The authors declare no competing financial interest.

■ ACKNOWLEDGMENTS

The authors thank Prof. Theresa McCormick for valuable discussions about tellurorosamine dyes and Dr. Samantha MacMillan for collecting the X-ray diffraction data for **Te(II)**. Diffraction data for **Te(IV)-Cl$_2$** were collected at the ChemMatCARS Beamline 15ID-D at Advanced Photon Source, Argonne National Laboratory. The authors thank Dr. Yu-Sheng Chen and Dr. Tieyan Chang for assisting in data collection. ChemMatCARS Sector 15 is supported by the NSF under Grant NSF/CHE-1834750. This research used resources of the Advanced Photon Source, a U.S. Department of Energy (DOE) Office of Science User Facility, operated for the DOE Office of Science by Argonne National Laboratory under Contract DE-AC02-06CH11357. N.K., M.R.C., and L.E.R. thank Daoyang Zhang who assisted with beamline data collection.

■ REFERENCES

(1) Lin, T.-P.; Gabbaï, F. P. Two-Electron Redox Chemistry at the Dinuclear Core of a TePt Platform: Chlorine Photoreductive Elimination and Isolation of a TeVPtI Complex. *J. Am. Chem. Soc.* **2012**, *134* (29), 12230−12238.

(2) Kieser, J. M.; Jones, L. O.; Lin, N. J.; Zeller, M.; Schatz, G. C.; Bart, S. C. Synthesis and Characterization of Tellurium Catecholates and Their N-Oxide Adducts. *Inorg. Chem.* **2021**, *60* (5), 3460−3470.

(3) Pietrasiak, E.; Togni, A. Synthesis and Characterization of Fluorinated Hypervalent Tellurium Derivatives. *Organometallics* **2017**, *36* (19), 3750−3757.

(4) Princival, C. R.; Archilha, M. V. L. R.; Dos Santos, A. A.; Franco, M. P.; Braga, A. A. C.; Rodrigues-Oliveira, A. F.; Correra, T. C.; Cunha, R. L. O. R.; Comasseto, J. V. Stability Study of Hypervalent Tellurium Compounds in Aqueous Solutions. *ACS Omega* **2017**, *2* (8), 4431−4439.

(5) Biot, N.; Romito, D.; Bonifazi, D. Substituent-Controlled Tailoring of Chalcogen-Bonded Supramolecular Nanoribbons in the Solid State. *Cryst. Growth Des.* **2021**, *21* (1), 536−543.

(6) Werz, D. B.; Gleiter, R.; Rominger, F. Nanotube Formation Favored by Chalcogen-Chalcogen Interactions. *J. Am. Chem. Soc.* **2002**, *124* (36), 10638−10639.

(7) Torubaev, Y. V.; Rozhkov, A. V.; Skabitsky, I. V.; Gomila, R. M.; Frontera, A.; Kukushkin, V. Y. Heterovalent chalcogen bonding: supramolecular assembly driven by the occurrence of a tellurium(ii)···Ch(i) (Ch = S, Se, Te) linkage. *Inorg. Chem. Front.* **2022**, *9* (21), 5635−5644.

(8) Duan, H.-Y.; Han, S.-T.; Zhan, T.-G.; Liu, L.-J.; Zhang, K.-D. Visible-Light-Switchable Tellurium-Based Chalcogen Bonding: Photocontrolled Anion Binding and Anion Abstraction Catalysis. *Angew. Chem., Int. Ed.* **2023**, *62* (5), e202212707.

(9) Guleria, A.; Gandhi, V. V.; Kunwar, A.; Debnath, A. K.; Adhikari, S. Highly stable spherical shaped and blue photoluminescent cyclodextrin-coated tellurium nanocomposites prepared by in situ generated solvated electrons: a rapid green method and mechanistic and anticancer studies. *Dalton Trans.* **2022**, *51* (16), 6366−6377.

(10) Chivers, T.; Laitinen, R. S. Tellurium: a maverick among the chalcogens. *Chem. Soc. Rev.* **2015**, *44* (7), 1725−1739.

(11) Cremer, C.; Goswami, M.; Rank, C. K.; de Bruin, B.; Patureau, F. W. Tellurium(II)/Tellurium(III)-Catalyzed Cross-Dehydrogenative C-N Bond Formation. *Angew. Chem., Int. Ed.* **2021**, *60* (12), 6451−6456.

(12) Wonner, P.; Steinke, T.; Vogel, L.; Huber, S. M. Carbonyl Activation by Selenium- and Tellurium-Based Chalcogen Bonding in a Michael Addition Reaction. *Chem. Eur. J.* **2020**, *26* (6), 1258−1262.

(13) Weiss, R.; Aubert, E.; Pale, P.; Mamane, V. Chalcogen-Bonding Catalysis with Telluronium Cations. *Angew. Chem., Int. Ed.* **2021**, *60* (35), 19281−19286.

(14) Fernández-Lodeiro, J.; Pinatto-Botelho, M. F.; Soares-Paulino, A. A.; Gonçalves, A. C.; Sousa, B. A.; Princival, C.; Dos Santos, A. A. Synthesis and biological properties of selenium- and tellurium-containing dyes. *Dyes Pigm.* **2014**, *110*, 28−48.

(15) Fan, F.; Wang, L.; Li, F.; Fu, Y.; Xu, H. Stimuli-Responsive Layer-by-Layer Tellurium-Containing Polymer Films for the Combination of Chemotherapy and Photodynamic Therapy. *ACS Appl. Mater. Interfaces* **2016**, *8* (26), 17004−17010.

(16) Lin, Y.; Wu, Y.; Wang, R.; Tao, G.; Luo, P.-F.; Lin, X.; Huang, G.; Li, J.; Yang, H.-H. Two-dimensional tellurium nanosheets for photoacoustic imaging-guided photodynamic therapy. *Chem. Commun.* **2018**, *54* (62), 8579−8582.

(17) Detty, M. R.; Merkel, P. B. Chalcogenapyrylium dyes as potential photochemotherapeutic agents. Solution studies of heavy atom effects on triplet yields, quantum efficiencies of singlet oxygen generation, rates of reaction with singlet oxygen, and emission quantum yields. *J. Am. Chem. Soc.* **1990**, *112* (10), 3845−3855.
(18) Yang, T.; Ke, H.; Wang, Q.; Tang, Y. a.; Deng, Y.; Yang, H.; Yang, X.; Yang, P.; Ling, D.; Chen, C.; Zhao, Y.; Wu, H.; Chen, H. Bifunctional Tellurium Nanodots for Photo-Induced Synergistic Cancer Therapy. *ACS Nano* **2017**, *11* (10), 10012−10024.
(19) Duhović, S.; Dincă, M. Synthesis and Electrical Properties of Covalent Organic Frameworks with Heavy Chalcogens. *Chem. Mater.* **2015**, *27* (16), 5487−5490.
(20) He, G.; Kang, L.; Torres Delgado, W.; Shynkaruk, O.; Ferguson, M. J.; McDonald, R.; Rivard, E. The Marriage of Metallacycle Transfer Chemistry with Suzuki-Miyaura Cross-Coupling To Give Main Group Element-Containing Conjugated Polymers. *J. Am. Chem. Soc.* **2013**, *135* (14), 5360−5363.
(21) Oyama, T.; Yang, Y. S.; Matsuo, K.; Yasuda, T. Effects of chalcogen atom substitution on the optoelectronic and charge-transport properties in picene-type π-systems. *Chem. Commun.* **2017**, *53* (27), 3814−3817.
(22) Jung, E. H.; Bae, S.; Yoo, T. W.; Jo, W. H. The effect of different chalcogenophenes in isoindigo-based conjugated copolymers on photovoltaic properties. *Polym. Chem.* **2014**, *5* (22), 6545−6550.
(23) Carrera, E. I.; Lanterna, A. E.; Lough, A. J.; Scaiano, J. C.; Seferos, D. S. A Mechanistic Study of Halogen Addition and Photoelimination from π-Conjugated Tellurophenes. *J. Am. Chem. Soc.* **2016**, *138* (8), 2678−2689.
(24) Carrera, E. I.; McCormick, T. M.; Kapp, M. J.; Lough, A. J.; Seferos, D. S. Thermal and Photoreductive Elimination from the Tellurium Center of π-Conjugated Tellurophenes. *Inorg. Chem.* **2013**, *52* (23), 13779−13790.
(25) Ashraf, R. S.; Meager, I.; Nikolka, M.; Kirkus, M.; Planells, M.; Schroeder, B. C.; Holliday, S.; Hurhangee, M.; Nielsen, C. B.; Sirringhaus, H.; McCulloch, I. Chalcogenophene Comonomer Comparison in Small Band Gap Diketopyrrolopyrrole-Based Conjugated Polymers for High-Performing Field-Effect Transistors and Organic Solar Cells. *J. Am. Chem. Soc.* **2015**, *137* (3), 1314−1321.
(26) Vallayil, P.; Sankararaman, S.; Ramanujam, K. Structurally and electrochemically tunable pyrylium platforms: A new class of redox anolyte for non-aqueous organic redox flow battery operating at a high-current density. *J. Energy Storage* **2023**, *58*, 106325.
(27) Calitree, B.; Donnelly, D. J.; Holt, J. J.; Gannon, M. K.; Nygren, C. L.; Sukumaran, D. K.; Autschbach, J.; Detty, M. R. Tellurium Analogues of Rosamine and Rhodamine Dyes: Synthesis, Structure, 125Te NMR, and Heteroatom Contributions to Excitation Energies. *Organometallics* **2007**, *26* (25), 6248−6257.
(28) Kryman, M. W.; Schamerhorn, G. A.; Yung, K.; Sathyamoorthy, B.; Sukumaran, D. K.; Ohulchanskyy, T. Y.; Benedict, J. B.; Detty, M. R. Organotellurium Fluorescence Probes for Redox Reactions: 9-Aryl-3,6-diaminotelluroxanthylium Dyes and Their Telluroxides. *Organometallics* **2013**, *32* (15), 4321−4333.
(29) Kryman, M. W.; Schamerhorn, G. A.; Hill, J. E.; Calitree, B. D.; Davies, K. S.; Linder, M. K.; Ohulchanskyy, T. Y.; Detty, M. R. Synthesis and Properties of Heavy Chalcogen Analogues of the Texas Reds and Related Rhodamines. *Organometallics* **2014**, *33* (10), 2628−2640.
(30) Mann, J. R.; Gannon, M. K.; Fitzgibbons, T. C.; Detty, M. R.; Watson, D. F. Optimizing the Photocurrent Efficiency of Dye-Sensitized Solar Cells through the Controlled Aggregation of Chalcogenoxanthylium Dyes on Nanocrystalline Titania Films. *J. Phys. Chem. C* **2008**, *112* (34), 13057−13061.
(31) McCormick, T. M.; Calitree, B. D.; Orchard, A.; Kraut, N. D.; Bright, F. V.; Detty, M. R.; Eisenberg, R. Reductive Side of Water Splitting in Artificial Photosynthesis: New Homogeneous Photosystems of Great Activity and Mechanistic Insight. *J. Am. Chem. Soc.* **2010**, *132* (44), 15480−15483.
(32) Lutkus, L. V.; Rettig, I. D.; Davies, K. S.; Hill, J. E.; Lohman, J. E.; Eskew, M. W.; Detty, M. R.; McCormick, T. M. Photocatalytic Aerobic Thiol Oxidation with a Self-Sensitized Tellurorhodamine Chromophore. *Organometallics* **2017**, *36* (14), 2588−2596.
(33) Rettig, I. D.; Van, J.; Brauer, J. B.; Luo, W.; McCormick, T. M. Tellurorhodamine photocatalyzed aerobic oxidation of organo-silanes and phosphines by visible-light. *Dalton Trans.* **2019**, *48* (17), 5665−5673.
(34) Clark, J. L.; Hill, J. E.; Rettig, I. D.; Beres, J. J.; Ziniuk, R.; Ohulchanskyy, T. Y.; McCormick, T. M.; Detty, M. R. Importance of Singlet Oxygen in Photocatalytic Reactions of 2-Aryl-1,2,3,4-tetrahydroisoquinolines Using Chalcogenorosamine Photocatalysts. *Organometallics* **2019**, *38* (12), 2431−2442.
(35) Koide, Y.; Kawaguchi, M.; Urano, Y.; Hanaoka, K.; Komatsu, T.; Abo, M.; Terai, T.; Nagano, T. A reversible near-infrared fluorescence probe for reactive oxygen species based on Te-rhodamine. *Chem. Commun.* **2012**, *48* (25), 3091−3093.
(36) Zheng, H.; Zhan, X.-Q.; Bian, Q.-N.; Zhang, X.-J. Advances in modifying fluorescein and rhodamine fluorophores as fluorescent chemosensors. *Chem. Commun.* **2013**, *49* (5), 429−447.
(37) Wang, L.; Du, W.; Hu, Z.; Uvdal, K.; Li, L.; Huang, W. Hybrid Rhodamine Fluorophores in the Visible/NIR Region for Biological Imaging. *Angew. Chem., Int. Ed.* **2019**, *58* (40), 14026−14043.
(38) Singh, A.; Dhau, J.; Kumar, R.; Badru, R.; Kaushik, A. Exploring the fluorescence properties of tellurium-containing molecules and their advanced applications. *Phys. Chem. Chem. Phys.* **2024**, *26* (13), 9816−9847.
(39) Rettig, I. D.; Halvorsen, K. M.; McCormick, T. M. Synthesis, photophysical characterization, and aerobic redox reactivity of electron-rich tellurorhodamine photocatalysts. *Dalton Trans.* **2023**, *52*, 3990−4001.
(40) Leonard, K. A.; Zhou, F.; Detty, M. R. Chalcogen(IV)-Chalcogen(II) Redox Cycles. 1. Halogenation of Organic Substrates with Dihaloselenium(IV) and -tellurium(IV) Derivatives. Dehalogenation of Vicinal Dibromides with Diaryl Tellurides. *Organometallics* **1996**, *15* (20), 4285−4292.
(41) *CrysAlisPro*; Oxford Diffraction /Agilent Technologies UK Ltd.: Yarnton, England, 2024.
(42) *APEX3*; Bruker-Nonius AXS Inc.: Madison, WI, 2016.
(43) Sheldrick, G. SHELXT - Integrated space-group and crystal-structure determination. *Acta Cryst. A* **2015**, *71* (1), 3−8.
(44) Sheldrick, G. Crystal structure refinement with SHELXL. *Acta Cryst. C* **2015**, *71* (1), 3−8.
(45) Dolomanov, O. V.; Bourhis, L. J.; Gildea, R. J.; Howard, J. A. K.; Puschmann, H. OLEX2: a complete structure solution, refinement and analysis program. *J. Appl. Crystallogr.* **2009**, *42* (2), 339−341.
(46) Del Valle, D. J.; Donnelly, D. J.; Holt, J. J.; Detty, M. R. 2,7-Bis-N,N-dimethylaminochalcogenoxanthen-9-ones via Electrophilic Cyclization with Phosphorus Oxychloride. *Organometallics* **2005**, *24* (15), 3807−3810.
(47) Rosch, L. E.; Crawley, M. R.; O'Donnell, R. M.; Rohrabaugh, T. N.; Ensley, T. R.; Sobiech, T. A.; Cook, T. R. Shining Light on the Solution- and Excited-State Dynamics of Chalcogenopyrylium Polymethine Dyes. *Organometallics* **2022**, *41* (16), 2301−2316.
(48) Čížková, M.; Cattiaux, L.; Mallet, J.-M.; Labbé, E.; Buriez, O. Electrochemical switching fluorescence emission in rhodamine derivatives. *Electrochim. Acta* **2018**, *260*, 589−597.
(49) Shida, N.; Nishiyama, H.; Zheng, F.; Ye, S.; Seferos, D. S.; Tomita, I.; Inagi, S. Redox chemistry of π-extended tellurophenes. *Commun. Chem.* **2019**, *2* (1), 124.
(50) Send, R.; Valsson, O.; Filippi, C. Electronic Excitations of Simple Cyanine Dyes: Reconciling Density Functional and Wave Function Methods. *J. Chem. Theory Comput.* **2011**, *7* (2), 444−455.
(51) Le Guennic, B.; Jacquemin, D. Taking Up the Cyanine Challenge with Quantum Tools. *Acc. Chem. Res.* **2015**, *48* (3), 530−537.

https://doi.org/10.1021/acs.inorgchem.4c01077
Inorg. Chem. 2024, 63, 13157−13165